OPTICA

Full-Stokes polarimetric measurements and imaging using a fractal superconducting nanowire single-photon detector

Nan Hu,[1,2,†] Yun Meng,[1,2,†] Kai Zou,[1,2] Yifan Feng,[1,2] Zifan Hao,[1,2] Stephan Steinhauer,[3] Samuel Gyger,[3] Val Zwiller,[3] and Xiaolong Hu[1,2,*]

[1]School of Precision Instrument and Optoelectronic Engineering, Tianjin University, Tianjin, 300072, China
[2]Key Laboratory of Optoelectronic Information Science and Technology, Ministry of Education, Tianjin, 300072, China
[3]Department of Applied Physics, Royal Institute of Technology (KTH), SE-106 91 Stockholm, Sweden
*Corresponding author: xiaolonghu@tju.edu.cn

Measuring the states of polarization (SoP) of light is fundamentally important for applications ranging from communication, sensing, spectroscopy, imaging, to navigation. Superconducting nanowire single-photon detectors (SNSPDs) are ideal detectors of choice for faint-light detection and measurements, but SNSPDs themselves cannot resolve the SoP of photons. Here, based on a fractal SNSPD, we demonstrate a full-Stokes polarimetric measurement system that can measure arbitrary SoP of faint light. The measured SoPs are in excellent agreement with those of a state-of-the-art commercial polarimeter, but the sensitivity of our system reaches -86.6 dBm, which is 26.6 dB better than that of the commercial counterpart. As a direct application, we further demonstrate remote polarimetric imaging (i.e., polarimetric LiDAR) with a complete set of polarimetric contrast. © 2022 Optica Publishing Group under the terms of the Optica Open Access Publishing Agreement

1. INTRODUCTION

Polarization is a fundamental property of light, which describes the vectorial nature of the electrical-field oscillation and represents a degree of freedom of light, in addition to its frequency, intensity, and spatial and temporal modes [1]. In nature, some insects can sense the states of polarization (SoP) of scattered sunlight or moonlight in atmosphere for navigation [2,3]. In scientific and technological applications, polarization measurements have been widely used in the telecommunications [4], imaging [5], spectroscopy [6], sensing [7], quantum entanglement [8], navigation [9], and astronomy [10,11]. Therefore, polarimetry has been extensively explored [5,7,12–18]; in particular, a significant amount of recent research effort has been focusing on making in-line and integrated polarimeters using metasurfaces [15], metallic plasmonic structures [17,19], and integrated photonic circuits [13,14]. In the faint-light regime and photon-starved applications, traditional polarimetry would not be competent due, mainly, to the limited sensitivity of the photodetectors. Single-photon detectors, for example, silicon single-photon avalanche diodes (SPADs), have been used in polarimetric observations and studies of black holes and pulsars [10,11], and they have also been used in airborne and space-based polarimetric LiDARs [20,21].

Superconducting nanowire single-photon detectors (SNSPDs) have in recent years attracted tremendous research interest, since they were invented in 2001 [22]. Now they have outperformed

other photon-counting technologies at infrared telecommunication wavelengths, and they are considered ideal detectors of choice for faint-light detection and measurements, with their sensitivity down to the single-photon level. They have been widely used in applications ranging from quantum-key distribution [23], quantum computation [24], LiDAR [25], to biomedical sensing [26]. Although SNSPDs exhibit the merits of high system detection efficiency (SDE) [27–30], high counting rate in the free-running mode [31], low dark count rate (DCR) [32], and low timing jitter [33], these detectors themselves cannot resolve the SoP of light or photons. Recently, Sun *et al.* made progress along this avenue and successfully demonstrated a four-quadrant polarization-sensitive SNSPDs for resolving linear SoP and imaging at the wavelength of 1550 nm [12]. However, to date, full-Stokes polarimetric measurements for arbitrary SoP of light in the faint-light regime using SNSPDs are still absent. Full-Stokes polarimetric measurements are important because, for example, in remote sensing and imaging, scattered light or echo photons from the objects are not necessarily in the linear SoP, but, generally, they could be elliptically polarized, partially polarized, or even unpolarized. Accurate measurements of arbitrary SoP in the faint-light regime can help obtain more types of polarimetric contrast and reveal rich information about the structure, material composition, and texture of the objects, as well as the orientations of surfaces [5], and therefore they would have broad application space.

In this paper, we demonstrate photon-counting full-Stokes polarimetric measurement of arbitrary SoP on and inside the Poincaré sphere, using a single-element fractal SNSPD [34–37] with low polarization sensitivity. The measured SoP show excellent agreement with those measured by a Thorlabs polarimeter, but the sensitivity of our polarimetric system has reached −86.6 dBm, which is 26.6 dB better than the state-of-the-art commercial one. As a direct application, we further demonstrate remote full-Stokes polarimetric imaging at the telecommunication wavelength using a time-multiplexed scheme [8] and obtain images with a complete set of polarimetric contrast as well as time-of-flight (ToF) depth contrast. We believe that this work could impact many relevant fields and applications including remote sensing, meteorology, and imaging, where polarimetric measurements play the central roles.

2. MEASUREMENTS OF STOKES PARAMETERS

The method of our measurement is the division-of-amplitude (DoA) polarimetry [18], which generally consists of two steps: (1) measurement and determination of the instrument matrix $\mathbf{F}$ of the DoA optical system and (2) measurement of the count rates by the SNSPD and determination of the full-Stokes SoP of the input faint light.

Figure 1(a) presents the schematics of the experimental setup, which consist of two parts: (1) the DoA optical system, shown in the purple dashed box, and (2) the polarization-insensitive fractal SNSPD system [34–37]. The input light was from a femtosecond fiber laser, with a repetition rate of 82 MHz, a central wavelength at 1560 nm, and average optical power of 17 dBm. After attenuated and collimated, the input light entered the DoA optical system and was split into four channels. Without attenuation, its SoPs were directly measured by a commercial polarimeter from Thorlabs (PAX1000IR2/M), whose dynamic range was from −60 to 10 dBm, according to its specification [38]. A piece of single-mode fiber (SMF) after the first beam splitter (BS) was for spatial filtering, which was necessary for polarimetric imaging as we will present later. Four linear polarizers (P) were placed between the collimators and the beam splitters with orientation angles of 0°, 90°, 45°, and 135°. The 0° axis is horizontal and in parallel with the optical table. A quarter-wave plate (QWP) was used between the beam splitter and the 135° polarizer, with its fast axis aligned to 0°. The four channels were combined into a single-mode fiber by a 4 × 1 fiber coupler and then were sent into the fiber-coupled fractal SNSPD.

The fractal SNSPD, made of NbTiN, was the key element in our setup, and it featured high SDE, low polarization sensitivity, and high timing resolution [34,35]. The fractal design aimed to eliminate the polarization dependence of SDE that commonly used meandering SNSPD exhibited [27–30] while preserving other major merits of SNSPDs. The reduced polarization sensitivity originated from the fractal topology of the nanowires. Figure 1(b) presents its false-colored scanning-electron micrograph (SEM) and the equivalent electrical circuit [34]. The white dashed box shows a second-order Peano fractal structure, and the entire device is composed of 64 such structures, electrically connected into a 16 cascaded unit, each with a two superconducting nanowire avalanche photodetector (16-2SNAP) [34]. The chip was etched into a keyhole shape for self-aligned packaging. For this particular device, Fig. 1(c) presents the polarization-maximum SDE (SDE$_{\text{max}}$) and polarization-minimum SDE (SDE$_{\text{min}}$) at the base temperature of 2.1 K, at the wavelength of 1560 nm, and with false

counts subtracted. The fractal SNSPD was biased at 19.17 µA throughout this work; at this bias current, SDE$_{\text{max}} = 69.9\%$, SDE$_{\text{min}} = 68.4\%$, the resulting polarization sensitivity was 1.02. Section I in Supplement 1 details the characterization of this fractal SNSPD system.

First, we determined the instrument matrix $\mathbf{F}$ of the DoA optical system. To do so, we used 18 polarization states on the Poincaré sphere with known (measured by the Thorlabs polarimeter) Stokes vectors $\mathbf{X}'_i = [1, S_1'^{i}, S_2'^{i}, S_3'^{i}]^{\text{T}}$ ($i = 1, 2, ..., 18$), including linear polarization states as well as left- and right-handed circular and elliptical polarization states [16]. For each polarization, we measured and calculated the normalized optical power in the four output ports $\mathbf{Y}_i = [\tilde{P}_0^i, \tilde{P}_{90}^i, \tilde{P}_{45}^i, \tilde{P}_{135}^i]^{\text{T}}$ ($i = 1, 2, ..., 18$), using the setup presented in Fig. S2 (see Section II in Supplement 1), where $\tilde{P}_j^i$ ($i = 1, 2, ..., 18$, $j = 0, 45, 90, 135$) is the optical power of output ports P_j^i, normalized to optical power of input light P_{in}^i. In these measurements, P_{in}^i was controlled to be between 0.14 and 10.75 dBm. We obtained $\mathbf{F}$ by solving the least-squares problem $\mathbf{Y}_i = \mathbf{F}\mathbf{X}'_i$ ($i = 1, 2, ..., 18$). The concrete expression of $\mathbf{F}$ is presented in Eq. S1 (see Section II in Supplement 1). To evaluate the accuracy of $\mathbf{F}$, we recalculated $\mathbf{X}_i = [1, S_1^i, S_2^i, S_3^i]^{\text{T}}$ by $\mathbf{F}^{-1}\mathbf{Y}_i = S_0^i \mathbf{X}_i$ and compared $\mathbf{X}_i$ with $\mathbf{X}'_i$. We use the distance between $\mathbf{X}_i$ and $\mathbf{X}'_i$, $\Delta_i = \sqrt{(S_1^i - S_1'^i)^2 + (S_2^i - S_2'^i)^2 + (S_3^i - S_3'^i)^2}$ ($i = 1, 2, ..., 18$), to quantify the error. We found that the error is within 0.03; or, on average, the error of each S parameter is approximately $\Delta/\sqrt{3} = 0.017$ (Table S1 in Section II in Supplement 1).

Then we used the experimental setup in Fig. 1(a) to measure the Stokes parameters, in particular, in the faint-light regime where the Thorlabs polarimeter became incompetent due to its limited sensitivity. We further attenuated the input light by approximately 70 to 80 dB so that P_{in}^i was controlled to be between −80.17 and −85.16 dBm. Table S2 of Supplement 1 lists the count rate of the fractal SNSPD at each polarization state. The integration time was 5 s for measuring the completely polarized light and 10 s for measuring the partially polarized and completely unpolarized light. We alternatively measured the count rates of each of the four channels with the other three channels blocked, obtaining the vector $\mathbf{Y}_i = [\text{CR0}^i, \text{CR90}^i, \text{CR45}^i, \text{CR135}^i]^{\text{T}}$. The Stokes vector of the input light at the wavelength of 1560 nm was calculated by $\mathbf{F}^{-1}\mathbf{Y}_i = S_0'^i [1, S_1'^i, S_2'^i, S_3'^i]^{\text{T}} = S_0'^i \mathbf{X}_i$. To test the effectiveness of our method, we generated 50 SoP, including completely and partially polarized states as well as the unpolarized state. Section III in Supplement 1 details the method for generating these states. We compared the Stokes parameters S_1^i, S_2^i, S_3^i ($i = 1, 2, ..., 50$) measured by the SNSPD polarimetric system and $S_1'^i, S_2'^i, S_3'^i$ ($i = 1, 2, ..., 50$) measured by the Thorlabs polarimeter. Figure 2 presents the results, and the full data set is presented in Section IV in Supplement 1. We quantified the difference between $\mathbf{X}_i = [1, S_1^i, S_2^i, S_3^i]^{\text{T}}$ and $\mathbf{X}'_i = [1, S_1'^i, S_2'^i, S_3'^i]^{\text{T}}$ by once again using the distance $\Delta_i = \sqrt{(S_1^i - S_1'^i)^2 + (S_2^i - S_2'^i)^2 + (S_3^i - S_3'^i)^2}$ ($i = 1, 2, ..., 50$). The largest distance was 0.12. Or, to better compare with other polarimeters reported in reference [19], on average, the error on each S parameter is approximately within $\Delta/\sqrt{3} = 0.069$. Based on the Stokes vectors $\mathbf{X}$ and $\mathbf{X}'$, we calculated $\text{DoP} = \sqrt{S_1^2 + S_2^2 + S_3^2}$, $\text{DoP}' = \sqrt{S_1'^2 + S_2'^2 + S_3'^2}$,
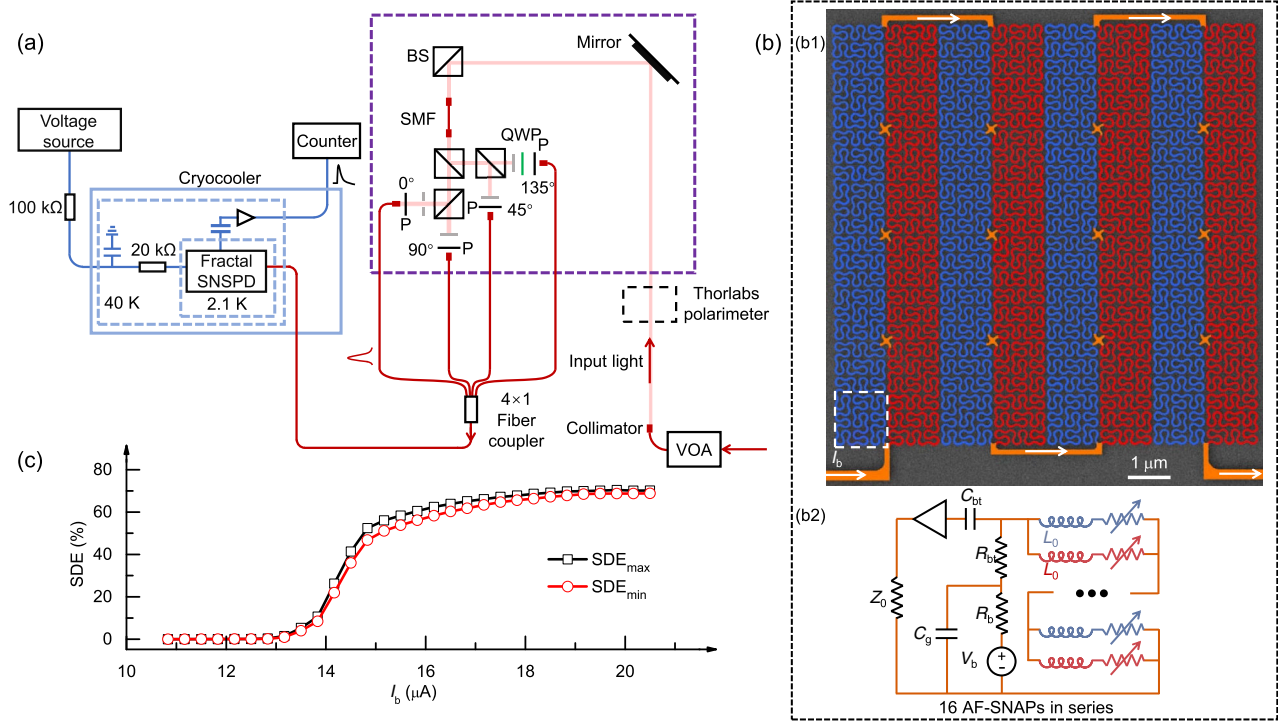
Fig. 1. Full-Stokes polarimetric measurements of faint light using a fractal SNSPD. (a) Schematics of the experimental setup. The instrument matrix **F** of the division-of-amplitude optical system in the purple dashed box was measured. The count rates of four channels, labeled as 0°, 90°, 45°, and 135°, were measured alternatively. The figure shows the configuration to measure the count rate in channel 0° with other three channels blocked. VOA, variable optical attenuator; BS, beam splitter; SMF, single-mode fiber; QWP, quarter-wave plate; P, linear polarizer. (b) False-colored scanning-electron micrograph and equivalent electrical circuit of the fractal SNSPD. (b1) A false-colored scanning-electron micrograph of the fractal SNSPD. The white dashed box shows a second-order Peano structure. The arrows show the direction of the flow of the supercurrent. (b2) Equivalent electrical circuit of the fractal SNSPD. (c) Measured polarization-maximum and minimum system detection efficiency (SDE) of the fractal SNSPD at the wavelength of 1560 nm.
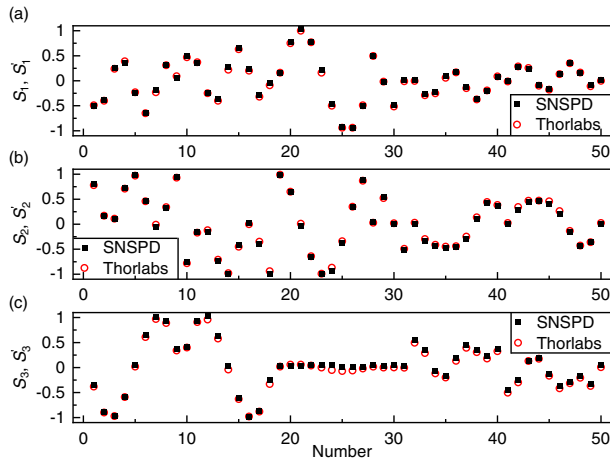
Fig. 2. Measured Stokes parameters (a) S_1, S_1'; (b) S_2, S_2'; and (c) S_3, S_3' by the SNSPD polarimetric system and the Thorlabs polarimeter. Note that light measured by the SNSPD polarimetric system was further attenuated by approximately 70 to 80 dB. These SoPs include completely polarized states, partially polarized states, and an unpolarized state.

$\text{DoLP} = \sqrt{S_1^2 + S_2^2}$, $\text{DoLP}' = \sqrt{S_1'^2 + S_2'^2}$, $\text{DoCP} = |S_3|$, $\text{DoCP}' = |S_3'|$, $\text{AoP} = 0.5 \arctan(S_2/S_1)$, and $\text{AoP}' = 0.5 \arctan(S_2'/S_1')$ as presented in Fig. S6 in Section IV in Supplement 1. We found excellent agreement between the measurements using the SNSPD polarimetric system and those using the Thorlabs polarimeter, except for the AoP for the circular

polarization states and the unpolarized state. The AoPs in these cases are not well defined because, theoretically, $S_1 = S_1' = 0$ and $S_2 = S_2' = 0$. To measure the sensitivity of the SNSPD polarimetric system, we kept decreasing the optical power of the input light. We found that the error Δ increased as the power decreased; see Section V in Supplement 1. We calculated the average error $\bar{\Delta}$ of the 50 SoP measurements and the standard deviation σ, and we defined the sensitivity as the optical power at which the error becomes $\bar{\Delta} + 3\sigma$. The sensitivity of the SNSPD polarimeter was measured to be -86.6 dBm.

3. POLARIMETRIC IMAGING

As a direct application of the photon-counting polarimeter, we reconfigured the experimental setup to perform polarimetric imaging as schematically shown in Fig. 3(a). The femtosecond fiber laser was still used as a light source. After split by a 90/10 fiber coupler, one channel, with 10% of light, went through a variable optical attenuator (VOA) and was detected by a fast photodetector. Its output provided the start signal for the time-to-amplitude converter (TAC). The other channel, with 90% of light, was collimated. The collimated beam passed through a linear polarizer and a 50/50 BS. It was steered by a beam-steering mirror (BSM) and illuminated the object, which was 3.5 m away from the BSM. Therefore, the setup was essentially configured as a polarimetric LiDAR. After replacing the mirror in Fig. 1(a) with the BSM in Fig. 3(a), we still assumed that the instrument matrix **F** for the DoA optical system in the purple dashed box remained the same. The
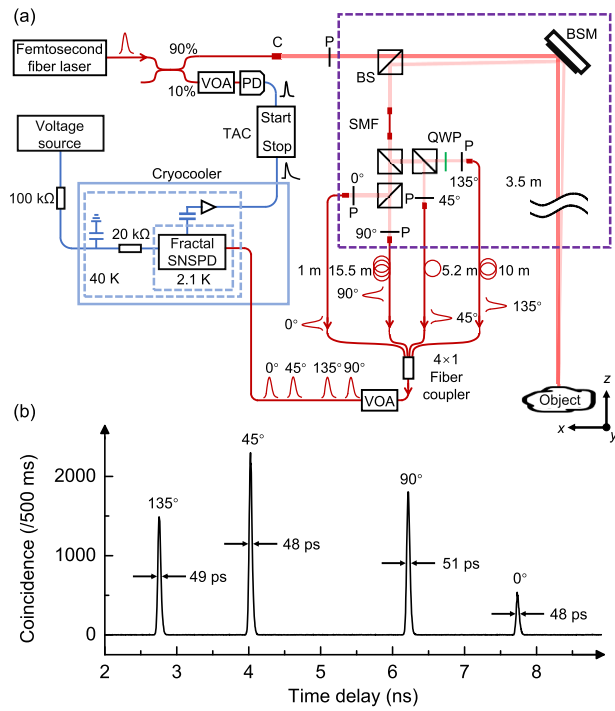
Fig. 3. Schematics of the division-of-amplitude polarimetric imaging system with a fractal SNSPD. (a) Schematics of the experimental setup. (b) An example histogram of the coincidences. VOA, variable optical attenuator; PD, photodetector; BS, beam splitter; BSM, beam-steering mirror; SMF, single-mode fiber; P, linear polarizer; QWP, quarter-wave plate; TAC, time-to-amplitude converter.

reflected light from the object went back and was coupled into a collimator connecting with the SMF for spatial filtering. We used a time-multiplexed scheme [8] to perform photon counting for four channels. To temporally separate the light in four channels, we used optical fibers with lengths of 1, 5.2, 10, and 15.5 m as delay lines. Light in four channels was combined by the 4×1 fiber coupler. After going through a VOA, light was sent to the fiber-coupled fractal SNSPD system. The output of the SNSPD system worked

as the stop signal for the TAC. The bin size of the TAC was set to be 4 ps. The light spot size at the object was approximately 5.2 mm, the step size of the raster scanning in the $x-y$ plane was 2 mm, and the dwell time for each pixel was 500 ms. Figure 3(b) presents an example histogram of the coincidences accumulated for 500 ms and the full widths at half-maxima of the Gaussian fitting to those peaks are between 48 and 51 ps.

Our experimental setup allows us to simultaneously obtain images with a full set of polarimetric contrast as well as ToF images. The first object we used is a dolly duck with its hairy body, a pair of plastic glasses, a cloth jacket, a metallic key and a chain, and a polyamide hat. The dolly duck was sitting on a plastic file box, and the background plate was made of bonded foam. Figure 4(a) shows the ground-truth photograph. Figures 4(b)–4(f) show the normalized intensity (i.e., $S_0 / S_0^{\max}$), CR0 (the photon counts with false counts subtracted in 500 ms in channel 0°), DoLP, DoCP, and AoP images, respectively. More polarimetric images with other types of contrast are presented in Section VI in Supplement 1. In Fig. 4(g), we fused the DoP and ToF images. We can see that the polarimetric as well as ToF images reveal rich information about the materials, texture, surface orientations, and profile of the object. For example, the body of the dolly duck exhibits relatively low DoP (and therefore, low DoLP and DoCP), showing the hairy feature that depolarizes light. In contrast, the plastic glasses, the metallic key, and the chain show high DoP as well as DoLP, making them easy to be identified. We note that in Fig. 4(g) some points show DoP slightly larger than 1, due to the measurement error of the instrument matrix **F**.

Polarimetric imaging provides additional contrasts in some applications in which ToF imaging fails. As an example, the second object we used is a papercut showing a Chinese character "Fu" (meaning good luck and good fortune) attached to a board. The thickness of the papercut was measured to be 0.2 mm, too thin to be resolved by ToF. Figure 5(a) presents the false-color DoP image, clearly showing the papercut. In comparison, in the ToF image presented in Fig. 5(b), the papercut is not recognizable. Section VI in Supplement 1 presents additional polarimetric images with other types of contrast as well as the ground-truth photograph.
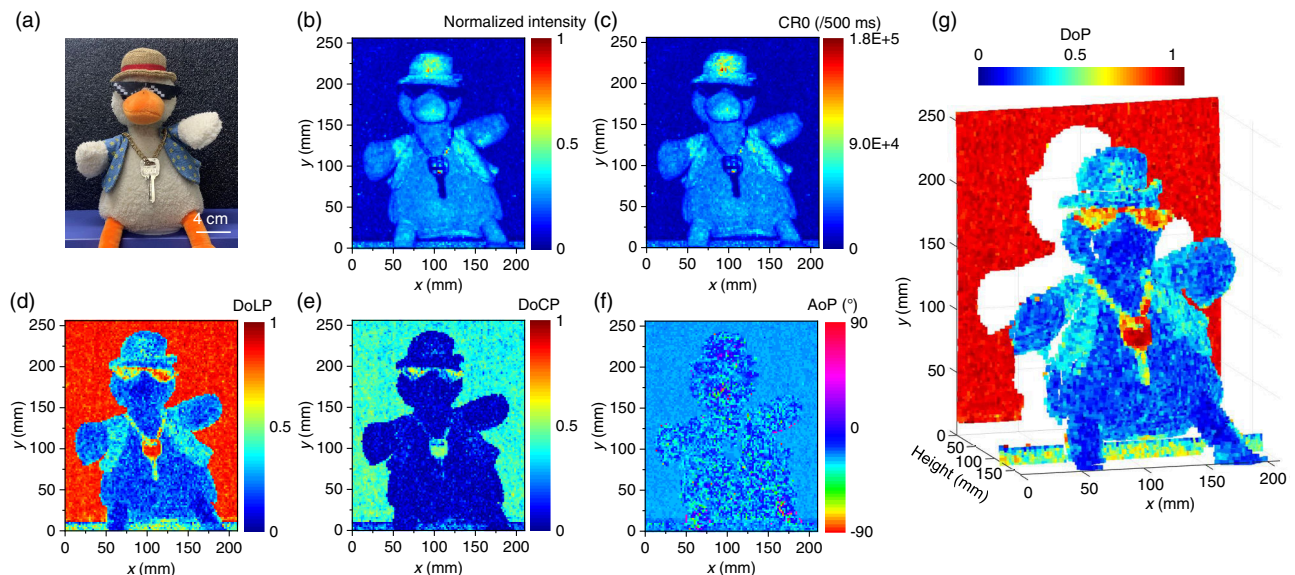
Fig. 4. Full-Stokes polarimetric and time-of-flight (ToF) images of a dolly duck. (a) Photograph; (b) false-color normalized intensity image; (c) false-color CR0 image; (d) false-color DoLP image; (e) false-color DoCP image; (f) false-color AoP image; (g) fused DoP and ToF image.
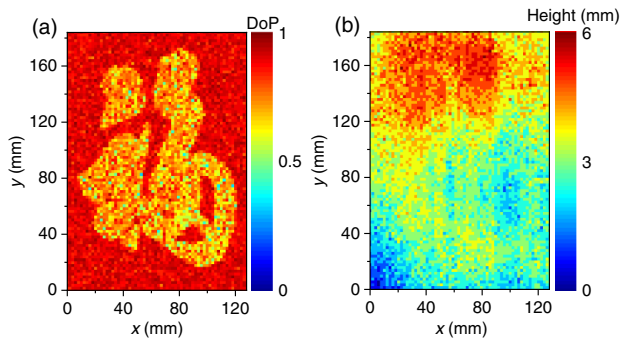
Fig. 5. Polarimetric and ToF images of a papercut attached on a board. (a) DoP image of the papercut. (b) ToF image of the papercut.

4. CONCLUSION

In summary, we have demonstrated full-Stokes polarimetric measurements and imaging at the wavelength of 1560 nm using a fractal SNSPD. The full-Stokes measurements of SoP of light showed excellent agreement with those of the state-of-the-art commercial polarimeter; however, our system exceeded in its sensitivity by 26.6 dB, reaching -86.6 dBm. For imaging, the full set of polarimetric contrast provided important information about the texture, materials, and surface orientations of the objects and presented objects that ToF imaging fails to discern.

We believe that this work will not only find direct applications in remote sensing and metrology, but also, based on this work, several extensions are possible to further enhance the functionality of the system and broaden its application space: (1) An array of polarization-insensitive fractal SNSPDs can be integrated with metasurfaces to avoid using the free-space optics so that the insertion loss could be minimized, the sensitivity could be further enhanced [19], and the footprint and weight of the optical setup could be reduced. Waveguide-integrated SNSPDs [39,40] can be combined with the miniature polarimeters based on integrated photonic circuits [13,14] to similarly minimize the insertion loss and reduce the footprint and weight of the optical setup. (2) The system can be further extended to a longer-distance one, maybe also for applications in foggy environment and underwater [7]. (3) The system, after necessary reconfiguration, can be applied in polarimetric microscopy [5]. (4) Polarimetric imaging can be extended to other technologically interesting wavelengths, thanks to the broad-spectrum single-photon sensitivity of SNSPDs. (5) Computational imaging and deep learning can be combined with this photon-counting polarimetric imaging system to find more applications [41,42].

Disclosures. The authors declare no conflicts of interest.

Data availability. Data underlying the results presented in this paper are not publicly available at this time but may be obtained from the authors upon reasonable request.

Supplemental document. See Supplement 1 for supporting content.

†These authors contributed equally to this paper.

REFERENCES AND NOTES

1. E. Wolf, *Introduction to the Theory of Coherence and Polarization of Light* (Cambridge University, 2007).
2. M. Dacke, D.-E. Nilsson, C. H. Scholtz, M. Byrne, and E. J. Warrant, "Insect orientation to polarized moonlight," Nature **424**, 33 (2003).
3. T. Labhart and E. P. Meyer, "Neural mechanisms in insect navigation: polarization compass and odometer," Curr. Opin. Neurobiol. **12**, 707–714 (2002).
4. S. X. Wang and A. Weiner, "Fast wavelength-parallel polarimeter for broadband optical networks," Opt. Lett. **29**, 923–925 (2004).
5. F. Snik, J. Craven-Jones, M. Escuti, S. Fineschi, D. Harrington, A. De Martino, D. Mawet, J. Riedi, and J. S. Tyo, "An overview of polarimetric sensing techniques and technology with applications to different research fields," Proc. SPIE **9099**, 90990B (2014).
6. B. Ranjbar and P. Gill, "Circular dichroism techniques: biomolecular and nanostructural analyses-a review," Chem. Biol. Drug Des. **74**, 101–120 (2009).
7. J. S. Tyo, D. L. Goldstein, D. B. Chenault, and J. A. Shaw, "Review of passive imaging polarimetry for remote sensing applications," Appl. Opt. **45**, 5453–5469 (2006).
8. T. Zhong, X. Hu, F. N. Wong, K. K. Berggren, T. D. Roberts, and P. Battle, "High-quality fiber-optic polarization entanglement distribution at 1.3 μm telecom wavelength," Opt. Lett. **35**, 1392–1394 (2010).
9. D. Lambrinos, R. Möller, T. Labhart, R. Pfeifer, and R. Wehner, "A mobile robot employing insect strategies for navigation," Robot. Auton. Syst. **30**, 39–64 (2000).
10. P. Collins, G. Kyne, D. Lara, M. Redfern, A. Shearer, and B. Sheehan, "The Galway astronomical Stokes polarimeter: an all-Stokes optical polarimeter with ultra-high time resolution," Exp. Astron. **36**, 479–503 (2013).
11. G. Kanbach, A. Stefanescu, S. Duscha, M. Mühlegger, F. Schrey, H. Steinle, A. Slowikowska, and H. Spruit, "OPTIMA: a high time resolution optical photo-polarimeter," in *High Time Resolution Astrophysics* (Springer, 2008), pp. 153–169.
12. X.-Q. Sun, W.-J. Zhang, C.-J. Zhang, L.-X. You, G.-Z. Xu, J. Huang, H. Zhou, H. Li, Z. Wang, and X.-M. Xie, "Polarization resolving and imaging with a single-photon sensitive superconducting nanowire array," Opt. Express **29**, 11021–11036 (2021).
13. W. Liu, J. Liao, Y. Yu, and X. Zhang, "High-efficient and high-accurate integrated division-of-time polarimeter," APL Photon. **6**, 071302 (2021).
14. Z. Lin, L. A. Rusch, Y. Chen, and W. Shi, "Optimal ultra-miniature polarimeters in silicon photonic integrated circuits," APL Photon. **4**, 100806 (2019).
15. J. B. Mueller, K. Leosson, and F. Capasso, "Ultracompact metasurface in-line polarimeter," Optica **3**, 42–47 (2016).
16. C. He, J. Chang, Y. Wang, R. Liao, H. He, N. Zeng, and H. Ma, "Linear polarization optimized Stokes polarimeter based on four-quadrant detector," Appl. Opt. **54**, 4458–4463 (2015).
17. F. Afshinmanesh, J. S. White, W. Cai, and M. L. Brongersma, "Measurement of the polarization state of light using an integrated plasmonic polarimeter," Nanophotonics **1**, 125–129 (2012).
18. R. Azzam, "Division-of-amplitude photopolarimeter (DOAP) for the simultaneous measurement of all four Stokes parameters of light," Opt. Acta **29**, 685–689 (1982).
19. A. Basiri, X. Chen, J. Bai, P. Amrollahi, J. Carpenter, Z. Holman, C. Wang, and Y. Yao, "Nature-inspired chiral metasurfaces for circular polarization detection and full-Stokes polarimetric measurements," Light Sci. Appl. **8**, 78 (2019).
20. P. Dabney, D. Harding, J. Abshire, T. Huss, G. Jodor, R. Machan, J. Marzouk, K. Rush, A. Seas, C. Shuman, X. Sun, S. Valett, A. Vasilyev, A. Yu, and Y. Zheng, "The slope imaging multi-polarization photon-counting lidar: development and performance results," in *IEEE International Geoscience and Remote Sensing Symposium*, IEEE, , 2010, pp. 653–656.
21. G. Acconcia, A. Giudici, J. A. Smith, I. Labanca, R. J. Hare, M. Ghioni, and I. Rech, "Toward high-performance SPAD arrays for space-based atmosphere and ocean profiling LiDARs," J. Appl. Remote Sens. **15**, 017501 (2021).
22. G. N. Gol'tsman, O. Okunev, G. Chulkova, A. Lipatov, A. Semenov, K. Smirnov, B. Voronov, A. Dzardanov, C. Williams, and R. Sobolewski, "Picosecond superconducting single-photon optical detector," Appl. Phys. Lett. **79**, 705–707 (2001).

23. J.-P. Chen, C. Zhang, Y. Liu, C. Jiang, W. Zhang, X.-L. Hu, J.-Y. Guan, Z.-W. Yu, H. Xu, J. Lin, M.-J. Li, H. Chen, H. Li, L. You, Z. Wang, X.-B. Wang, Q. Zhang, and J.-W. Pan, "Sending-or-not-sending with independent lasers: secure twin-field quantum key distribution over 509 km," Phys. Rev. Lett. **124**, 070501 (2020).

24. H. S. Zhong, H. Wang, Y.-H. Deng, *et al.*, "Quantum computational advantage using photons," Science **370**, 1460–1463 (2020).

25. A. McCarthy, N. J. Krichel, N. R. Gemmell, X. Ren, M. G. Tanner, S. N. Dorenbos, V. Zwiller, R. H. Hadfield, and G. S. Buller, "Kilometer-range, high resolution depth imaging via 1560 nm wavelength single-photon detection," Opt. Express **21**, 8904–8915 (2013).

26. N. R. Gemmell, A. McCarthy, B. Liu, M. G. Tanner, S. D. Dorenbos, V. Zwiller, M. S. Patterson, G. S. Buller, B. C. Wilson, and R. H. Hadfield, "Singlet oxygen luminescence detection with a fiber-coupled superconducting nanowire single-photon detector," Opt. Express **21**, 5005–5013 (2013).

27. J. Chang, J. W. N. Los, J. O. Tenorio-Pearl, N. Noordzij, R. Gourgues, A. Guardiani, J. R. Zichi, S. F. Pereira, H. P. Urbach, V. Zwiller, S. N. Dorenbos, and I. E. Zadeh, "Detecting telecom single photons with $(99.5_{-2.07}^{+0.5})$% system detection efficiency and high time resolution," APL Photon. **6**, 036114 (2021).

28. D. V. Reddy, R. R. Nerem, S. W. Nam, R. P. Mirin, and V. B. Verma, "Superconducting nanowire single-photon detectors with 98% system detection efficiency at 1550 nm," Optica **7**, 1649–1653 (2020).

29. P. Hu, H. Li, L. You, H. Wang, Y. Xiao, J. Huang, X. Yang, W. Zhang, Z. Wang, and X. Xie, "Detecting single infrared photons toward optimal system detection efficiency," Opt. Express **28**, 36884–36891 (2020).

30. I. Esmaeil Zadeh, J. W. N. Los, R. B. M. Gourgues, *et al.*, "Efficient single-photon detection with 7.7 ps time resolution for photon correlation measurements," ACS Photon. **7**, 1780–1787 (2020).

31. W. Zhang, J. Huang, C. Zhang, L. You, C. Lv, L. Zhang, H. Li, Z. Wang, and X. Xie, "A 16-pixel interleaved superconducting nanowire single-photon detector array with a maximum count rate exceeding 1.5 GHz," IEEE Trans. Appl. Supercond. **29**, 2200204 (2019).

32. Y. Hochberg, I. Charaev, S.-W. Nam, V. Verma, M. Colangelo, and K. K. Berggren, "Detecting sub-GeV dark matter with superconducting nanowires," Phys. Rev. Lett. **123**, 151802 (2019).

33. B. Korzh, Q.-Y. Zhao, J. P. Allmaras, *et al.*, "Demonstration of sub-3 ps temporal resolution with a superconducting nanowire single-photon detector," Nat. Photonics **14**, 250–255 (2020).

34. Y. Meng, K. Zou, N. Hu, L. Xu, X. Lan, S. Steinhauer, S. Gyger, V. Zwiller, and X. Hu, "Fractal superconducting nanowires detect infrared single photons with 84% system detection efficiency, 1.02 polarization sensitivity, and 20.8 ps timing resolution," (submitted).

35. Y. Meng, K. Zou, N. Hu, X. Lan, L. Xu, J. Zichi, S. Steinhauer, V. Zwiller, and X. Hu, "Fractal superconducting nanowire avalanche photodetector at 1550 nm with 60% system detection efficiency and 1.05 polarization sensitivity," Opt. Lett. **45**, 471–474 (2020).

36. X. Chi, K. Zou, C. Gu, J. Zichi, Y. Cheng, N. Hu, X. Lan, S. Chen, Z. Lin, V. Zwiller, and X. Hu, "Fractal superconducting nanowire single-photon detectors with reduced polarization sensitivity," Opt. Lett. **43**, 5017–5020 (2018).

37. C. Gu, Y. Cheng, X. Zhu, and X. Hu, "Fractal-inspired, polarization-insensitive superconducting nanowire single-photon detectors," in *Novel Optical Materials and Applications* (Optical Society of America, 2015), paper JM3A.10.

38. https://www.thorlabs.com/thorproduct.cfm?partnumber=PAX1000IR2/M, 2021-12-16, The dynamic range was specified to be −60 dBm to +10 dBm. There was an additional note on the specification: "All polarization specifications are valid for power range from −40 dBm to +3 dBm."

39. X. Hu, C. W. Holzwarth, D. Masciarelli, E. A. Dauler, and K. K. Berggren, "Efficiently coupling light to superconducting nanowire single-photon detectors," IEEE Trans. Appl. Supercond. **19**, 336–340 (2009).

40. F. Najafi, J. Mower, N. C. Harris, F. Bellei, A. Dane, C. Lee, X. Hu, P. Kharel, F. Marsili, S. Assefa, K. K. Berggren, and D. Englund, "On-chip detection of non-classical light by scalable integration of single-photon detectors," Nat. Commun. **6**, 5873 (2015).

41. Y. Yang, Q. Yan, L. Tao, Y. Wang, D. Li, and Y. Wang, "Full Stokes single photon compressive polarization imaging," Rev. Sci. Instrum. **91**, 053701 (2020).

42. T. Liu, K. de Haan, B. Bai, Y. Rivenson, Y. Luo, H. Wang, D. Karalli, H. Fu, Y. Zhang, J. FitzGerald, and A. Ozcan, "Deep learning-based holographic polarization microscopy," ACS Photon. **7**, 3023–3034 (2020).